Available online at www.sciencedirect.com
SCIENCE DIRECT®
Surface and Coatings Technology 179 (2004) 279–285
SURFACE & COATINGS TECHNOLOGY
www.elsevier.com/locate/surfcoat

Nanocomposite layers of ceramic oxides and metals prepared by reactive gas-flow sputtering

M. Birkholz*, U. Albers, T. Jung

Fraunhofer Institut für Schicht-und Oberflächentechnik, Bienroder Weg 54 E, 38108 Braunschweig, Germany

Received 21 February 2003; accepted in revised form 14 July 2003

Abstract

Thin nanocomposite layers of ceramic oxides in conjunction with a second metallic phase were prepared by reactive gas-flow sputtering. The two nanogranular phases were dispersed into each other by co-deposition from two separate targets. TiO_2 and Al_2O_3 were chosen as ceramic phase, respectively, which was obtained by sputtering one of the metals and reacting with oxygen. In order to investigate the influence of a hard and a ductile metal, either tungsten or copper was chosen as the second metallic phase. Highly compact thin films could be prepared as was revealed by SEM. A low hydrogen content of 1–2 at.% was measured by SIMS indicating a low sample porosity and an effective residual gas displacement from the surface of the growing film. X-Ray diffraction revealed the TiO_2-derived films to contain rutile-phase grains of average grain size of less than 10 nm. Mechanical and tribological properties of the 3- to 4-μm thick coatings were determined by a micro-indenter operating with a Vickers-type diamond and by a pin-on-disk tester. The plastic microhardness HU_{pl} amounted up to 24.1 GPa in case of TiO_2-derived nanocomposite films and up to 14.8 GPa in case of Al_2O_3-based films. Also, with respect to tribological properties TiO_2:Cu and TiO_2:W coatings were superior over Al_2O_3-derived ones. A wear coefficient of 0.35×10^{-6} mm^3/Nm was obtained for optimised TiO_2 films against an alumina sphere under unlubricated sliding conditions. In lubricated pin-on-disk tests wear coefficients on the order of 0.1×10^{-6} mm^3/Nm were obtained for both metal-doped TiO_2 and Al_2O_3 films.

Keywords: Vickers hardness; Pin on disc; X-Ray diffraction; Reactive sputtering; Cermets and composites; Nanocomposites

1. Introduction

Hard coatings for wear and abrasive protection are mainly fabricated from nitride compounds and carbon-based compounds [1]. Their usage has enabled prolonged lifetimes of a large variety of sliding mechanical assemblies like engine working parts, rolling elements such as bearings, cutting tools and others [2]. For many applications in air or under humidity it would be desirable, however, to dispose of hard coatings that better withstand oxidation or corrosion under chemical attack. Oxides would accordingly represent an ideal class of materials for these purposes since they are stable at high temperatures and in chemically aggressive environments. Various oxide systems are currently under investigations with many activities focussing on the Al–O system [3,4] and the Zr–O system [5]. Two strategies might be applied to overcome the brittleness of ceramic oxides, which is the main obstacle for their use in tribological applications: one approach makes use of the change of mechanical properties with decreasing grain sizes down to the nanometer range [6], while in a second approach the dispersion of a second metallic phase into the granular ceramic material is used. In this work, we report on experiments that make equally use of both approaches by preparing nanogranular dispersions of metal–oxides and metals by virtue of the gas-flow sputtering (GFS) technique [7,8]. This deposition technique appears well suited for the preparation of nanogranular particles and coatings, since it operates in a pressure range where high collisional probabilities between the active species leads to the formation of nanometer-sized particles already in the gas–plasma phase [9]. The GFS process may be equally applied to the deposition of a large variety of metallic and metal–

*Corresponding author. Tel.: +49-531-2155626; fax: +49-531-2155900.
E-mail address: birkholz@ist.fhg.de (M. Birkholz).

0257-8972/04/$ - see front matter © 2003 Elsevier B.V. All rights reserved.
doi:10.1016/S0257-8972(03)00865-X

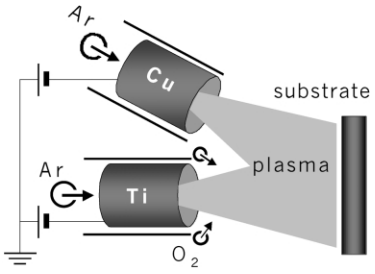

Fig. 1. Scheme of deposition geometry for a co-deposition experiment.

oxide coatings and high deposition rates of some 10 μm/h may be obtained for coatings of metal oxides. The technique is well suited for industrial applications, since it requires only a comparatively simple vacuum equipment and can be up-scaled to large areas [10]. For the study on nanocomposites presented here, TiO_2 and Al_2O_3 were chosen for the oxide phase, while Cu and W were chosen for the metallic matrix phase. The focus of this work was on the region of high oxide concentrations combined with less amounts of the metallic matrix phase. It will be shown that metal–oxide–metal coatings with high mechanical hardness and advantageous tribological properties can be prepared by the GFS technique.

2. Deposition process and preparation of nanoparticles by GFS

The GFS process operates in a pressure range of 0.1–1 mbar, which is 1–2 orders of magnitude higher than in the usual magnetron sputtering. This pressure regime is associated with short mean free paths of gas atoms in the 100-μm range and a viscous flow of gas, because of which the process has been named gas-flow sputtering [11]. The deposition technique makes use of the hollow cathode effect, which is associated with a high plasma density of 10^{12}–10^{13} cm^{-3} [12]. Thin films as presented in this work were produced with cylindrical targets through which a flow of argon gas was passed, see Fig. 1. These cylinders (∅ 40×60 mm) were operated as hollow cathode, i.e. as sputter cathode by applying a d.c. power in the range between 2 and 4 kW. The gas stream was conducted through the tubes to the substrate, which was positioned at a distance of 10 cm behind the tube openings. Most of the experiments were performed under a total pressure of 0.4 mbar. Pure oxygen gas was introduced into the gas stream after it had left the hollow cathode for the formation of metal–oxide nanoparticles.

The preparation of composite layers may be performed via different routes with the GFS technique. Our investigation concentrated on the co-deposition technique, which operates by running two hollow cathodes with different tube materials like Ti, Al, Cu and W, see Fig. 1. Cu-doped TiO_2 coatings, for instance, were prepared by directing one Ar stream through a Ti-tube GFS source and a second Ar stream through a Cu source to the substrate. Thin films were prepared on both CZ-Si (100) wafers and 100Cr6 steel shims. Before deposition the substrates were cleaned by a plasma-assisted process by biasing the substrate (−400 V) and passing an argon flow of 80 sccm through the chamber yielding a total pressure of approximately 0.05 mbar. The substrate was first coated with pure metal Ti or Al, respectively, to improve the adhesion of the functional layer. In a second step the oxygen flow was opened and the second hollow cathode was switched on for the preparation of the nanocomposite layer. In order to facilitate hard and compact coatings, the deposition process was supported by biasing the substrate (−100 V). No intentional heating of the substrate was applied, but temperatures up to 200 °C were measured at the back of the Si substrates during the process by virtue of an electrically isolated thermocouple. The ranges of deposition parameters investigated with the co-deposition technique are listed in Table 1. For most of the TiO_2- and Al_2O_3-derived nanocomposite coatings reported in the following, the Ti target or Al target was powered with 2.5 kW (equivalent to 33 W/cm^2), which was associated with voltages in the range between 650 and 700 V.

Transmission electron microscopy (TEM) was applied to study the ability of GFS for the preparation of nanogranular particles. For this purpose, very short

Table 1
Investigated ranges of deposition parameters during GFS co-deposition process for the preparation of nanocomposite oxide layers

Global parameters		
Total pressure	0.2–0.9 mbar	
Substrates	CZ-(100) Si wafer and 100Cr6	
Individual parameters	Ceramic particle phase	Metallic matrix phase
Material	TiO_2, Al_2O_3	Cu, W
Target powder density/W/cm^2	30–50	0–14
Cathode voltages/V	400–800	0–1000
Cathode currents/A	3.5–6.5	0–1
Argon flow/sccm	500–2000	50–800
Oxygen flow/sccm	1–80	–
Source-substrate distance/cm	6–20	10–15

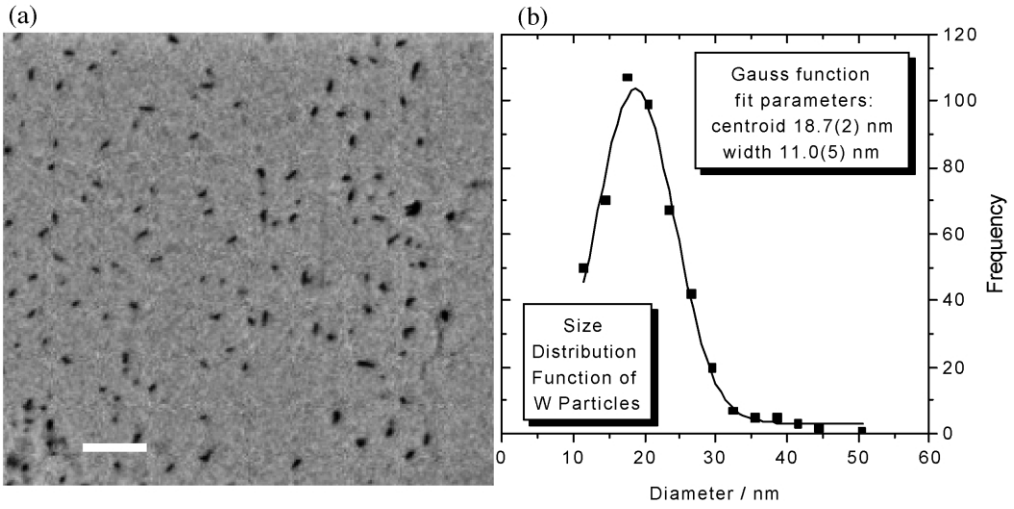

Fig. 2. (a) Transmission electron micrograph of tungsten particles produced by a 1 s gas-flow sputtering experiment, substrate: graphite-coated TEM grid. The bar in the lower left corner measures 200 nm. (b) Particle size distribution function of tungsten particles that was obtained by gauging the shape of 480 grains. The frequency of calculated diameters was well accounted for a by Gaussian function with peak centroid at 19 nm and a width of 11 nm.

deposition experiments of a duration of 1 s were performed in order to deposit the nanoparticles formed in the gas–plasma phase as isolated islands on the substrate. Such capture experiments are frequently applied to prepare a set of countable and measurable nanoparticles [13], from the measurement of which the particle size distribution function (PSDF) can be derived. Graphite-coated TEM grids (3.05 mm, 200 mesh) were positioned 12 cm in front of the target's aperture and 1200 sccm Ar were conducted through a W target that was powered with 3 kW. The sputtered metal atoms were swept out of the cathode with the Ar gas stream forming clusters during their transport to the TEM grids due to a high probability for direct collision under an exerted total pressure of 0.53 mbar. Fig. 2a displays a TEM micrograph from one of the grids showing a set of few dozen particles. Their chemical nature was investigated by electron spectroscopic imaging (ESI), unequivocally identifying the captured clusters to consist of tungsten. It is therefore concluded that W atoms had indeed formed nanoclusters during the transport from the sputter cathode to the substrate. The particle distribution function was derived by sizing the projected surface of 480 particles and calculating an average diameter for each. The obtained PSDF is shown in Fig. 2b. It was often observed that PSDF of nanometer-sized grain ensembles are well accounted for by a log-normal distribution function [14]. However, in the case presented in Fig. 2b a Gaussian function yielded smaller estimated S.D. and an increased reliability value when both model functions were fitted to the data. The average particle diameter is accordingly 18.7 ± 0.2 nm, while the width of the PSDF amounts to 11.0 ± 0.5 nm. This experiment clearly demonstrates the capability of the GFS technique to prepare nanogranular particles. Since all experiments were performed under comparable deposition conditions, it can be assumed that particle growth occurred in the gas–plasma phase yielding a nanogranular composition in the films prepared. The main deposition parameters by which the PSDF might be tailored are the total pressure, the electrical power conducted to the target and the distance between target and substrate.

3. Composition, morphology and mechanical properties

The stoichiometry of prepared samples was evaluated with an electron microscope analysis (EPMA) system by exciting with 12 keV electrons, and determining the integral intensity of the metals' and oxygen Kα emission line, against defined standards. By properly adjusting the deposition parameters metal oxide films close to the ideal stoichiometry were obtained, yielding for instance a O/Ti ratio of 2.02 ± 0.02 in case of pure titanium dioxide films. The concentration of the metals' matrix phase was varied in the range from 0 to 5 at.%. Fig. 3 displays a SEM cross-section micrograph of a slightly copper-doped TiO_2 film on Si, portraying a highly compact morphology without a noticeable columnar growth structure. Pure oxide films without matrix inclusions were optically transparent. SIMS measurements of Cu-doped and pure TiO_2 samples revealed a low hydrogen content in the 1–2 at.% range. This result is interpreted to indicate an effective residual gas displacement from the surface of the growing film, since otherwise, higher amounts of hydroxyl groups would have been built-in to the growing film. The expulsion

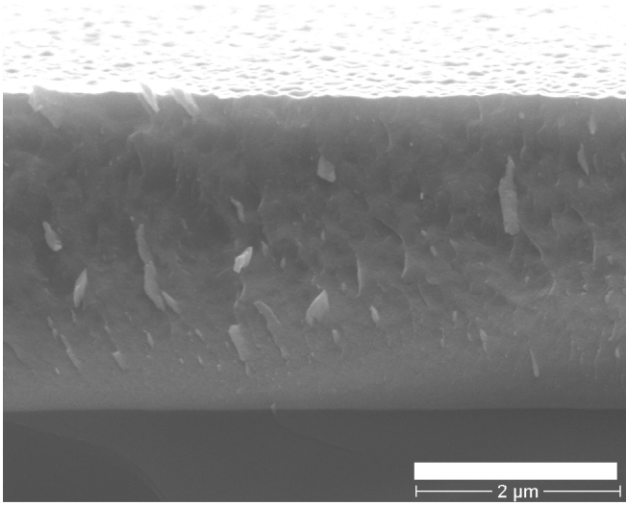

Fig. 3. SEM cross-sectional micrograph of copper-doped TiO_2 film prepared by reactive gas-flow sputtering. The film is recognized to be highly compact without columnar growth structures.

of residual gas from the active area is due to the argon stream onto the substrate and might be considered as a key element for the preparation of low-contaminated films in a rough vacuum environment. Moreover, the small hydrogen amount measured by SIMS, signals a low-porosity such that ex-situ H_2O contaminations from the ambient were successfully expelled and not incorporated into the films.

Hardness H and elastic modulus E were measured with a Fischerscope microindenter FH 100 according to the standard technical rules [15]. For this purpose a Vickers-shaped diamond pyramid was pressed into the coating by increasing the loading to a maximum force between 30 and 50 mN. The maximum indentation depth during the measurement was: (i) larger than 200 nm; (ii) smaller than or approximately 1/10 of the film thickness; (iii) exceeded the 20-fold R_a roughness of the coating [15]. The hardness was evaluated from the tangent to the unloading curve (plastic universal hardness HU_{pl}), so that Vickers hardness values HV could be derived from an established relationship [16] and the values obtained can directly be compared with other hard coatings, see for instance, for the nitride systems [17,18]. The hardness of the Al_2O_3-derived composite films was found in the 14–15 GPa range, which compares well with pure Al_2O_3 thin films prepared by other deposition techniques under the same temperature conditions [3]. The hardness values in the range of up to 24.1 GPa were obtained in the case of TiO_2-based coatings, which corresponds to a Vickers hardness of 2060 HV. This value was equally obtained for TiO_2 coatings prepared on steel shims and on silicon wafers. Table 2 lists the mechanical and some other properties of the prepared films. It can be seen that the microhardness is approximately 1/10 of the elastic modulus, which is typically observed for hard coatings and can be taken as justification for the reliability of obtained values. To our knowledge, such hard TiO_2 coatings have not been prepared before. Up to now, our investigations did not reveal a hardness enhancement caused by the inclusion of a metallic matrix phase as has generally been established to occur in the case of materials from the nitride system [17,18]. The highest hardness values were exhibited by pure oxides, from which especially the TiO_2 coatings show remarkable high hardness. The tribological properties of one set of the oxide layers (group of Al_2O_3-derived coatings), however, sensitively depended on the inclusion of a second metal matrix phase.

Tribological investigations of nanocomposite films were performed under dry-sliding and under lubricated conditions by use of a pin-on-disk tester. For this purpose, a stationary alumina (99.7%) sphere of 4.0-mm diameter (Saphirwerk, CH, grade 10) was pressed against the plane surface of the rotating specimen (30 rpm) by a normal force of $F_N = 2$ N and a sliding speed of 4 cm/s. The sliding distance was $D = 200$ m at a radius of 26 mm, resulting in more than 2500 cycles. Tests were performed under ambient conditions, i.e. under varying relative humidity that ranged from 44 to 62% for the different tests. The wear coefficient $K =$

Table 2
Mechanical and tribological properties of nanocomposite coatings prepared by reactive gas-flow sputtering (hardness and associated values: maximum values, pin-on-disk results: optimum range)

		TiO_2-based	Al_2O_3-based
Hardness/GPa		24.1	14.8
Equivalent to Vickers hardness/HV		2060	1300
Elastic modulus E/GPa		268	179
Elastic share of indentation work W_{el}/W_{tot}/%		59	53
Tribological pin-on-disk test vs. 4 mm Al_2O_3 sphere (sliding velocity 4 cm/s, load 2 N)			
Unlubricated	Coefficient of friction	0.4–0.5	0.6–0.8
	Wear coefficient $K/10^{-6}$ mm^3/Nm	0.3–0.4	8–10
Lubricated (0W30)	Coefficient of friction	0.13–0.14	0.11–0.13
	Wear coefficient $K/10^{-6}$ mm^3/Nm	<0.1	0.05–0.3

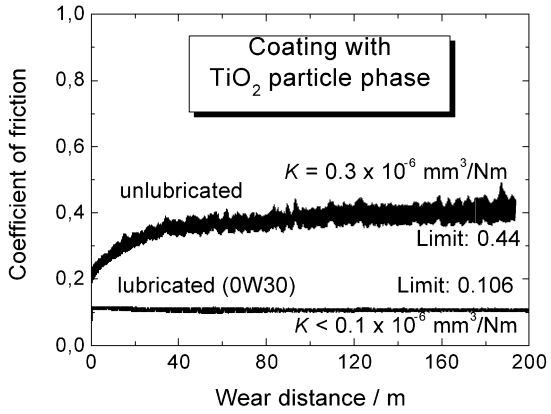

Fig. 4. Coefficient of friction vs. wear distance for lubricated (lower curve) and unlubricated (upper curve) pin-on-disk tests of TiO_2-based nanocomposite layers.

$V_w/D/F_N$ was derived from the worn volume V_w as determined from step profiling the wear track. Practically, for all tests under dry sliding conditions the same course of the coefficient of friction (*COF*) as a function of testing time was observed. The *COF* started with a value around or less than 0.2, but increased after some 100 cycles. The set of all samples decomposed into two groups, for the first of which the *COF* stabilized at constant values, while for the second set the coating became totally grinded after less than the total testing time. We interpret this phenomenon in terms of an abrasive wear mechanism with the wastage from the wear track acting as abrasive agent.

The coatings could be considered to decompose into a first group that withstand the wear from its own abraded material, while the second group does not. Pure Al_2O_3 coatings turned out to belong to the second group. In their case, the integration of Cu or W nanodispersions led equally to an enhanced stability against abrasive wear. Also, the extreme sensitivity of pure Al_2O_3 coatings against moisture was reduced by the inclusion of one of the metal matrix components. The coefficient of friction for Al_2O_3:Cu and Al_2O_3:W coatings were found in the 0.6–0.8 range, while the wear coefficients for the measuring conditions given above amounted to 8–10×10^{-6} mm^3/Nm. In case of TiO_2-derived nanocomposite coatings, improved tribological properties could be demonstrated as was expected because of their enhanced mechanical hardness. For coatings made from pure titanium dioxide the initial coefficient of friction (*COF*) amounted to 0.2, but raised to 0.5 after 50 m and stayed constant for the remaining sliding distance, see Fig. 4. The wear coefficient was determined to $K=0.35\times10^{-6}$ mm^3/Nm, which is at the low edge of measured values for unlubricated sliding ceramic–ceramic couples [19]. In case of the lubricated measurement with a standard motor oil (0W30), the wear coefficient was hardly measurable and only an upper limit of 0.1×10^{-6} mm^3/Nm can be specified.

The coefficient of friction of titanium oxides has been reported to decrease with increasing sliding velocity and increasing temperature [19]. Compared to the cited literature, the thin TiO_2 films presented in this work were examined with rather low sliding velocity of 4 cm/s and this may offer the potential for further tribological applications, where sliding velocities in the m/s range are often applied.

4. Structural characterisation

In order to gain more insight into the nanogranular morphology associated with gas-flow sputtered thin films and into the microscopic structure of such hard and wear resistant coatings the samples were examined by X-ray diffraction. The focus for these investigations was on TiO_2-based coatings because of their superior mechanical and tribological properties. For this purpose, a Seifert XRD 3000 PTS diffractometer equipped with a secondary graphite monochromator and operated with a copper anode [$\lambda(K\alpha_1)=154.0598$ pm] at 40 kV and 30 mA, was utilised in asymmetric grazing incidence (GI) geometry by setting the angle of incidence to $\alpha=0.3°$. Diffractograms were measured in the step scan mode and a step size of 0.05°. Fig. 5 displays the diffraction patterns as obtained for a 4.2 μm thin film deposited on a 100Cr6 steel shim. Inserted histograms display Bragg reflection positions and relative intensities for TiO_2 rutile and hexagonally-closed packed Ti powder samples according to ICDD (International Centre for Diffraction Data) card numbers 21-1276 and 5-682. The measured reflections are seen to be clearly accounted for by the rutile phase. The small deviations in scattering

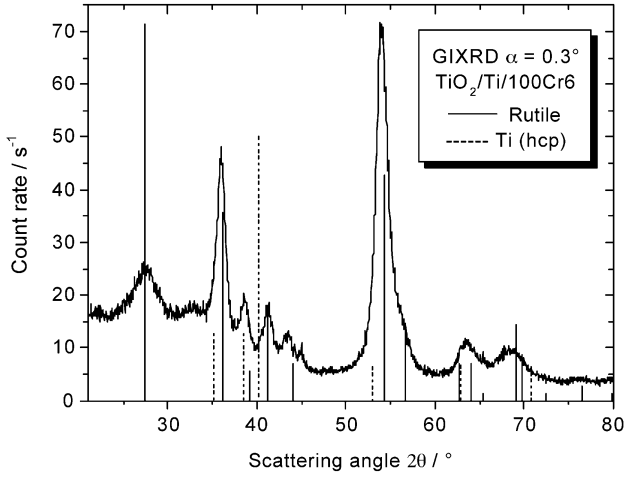

Fig. 5. X-Ray diffraction pattern of TiO_2/Ti/steel measured in grazing incidence geometry, $\alpha=0.3°$, with CuKα radiation. The sticks indicate positions and integral intensities of rutile and hcp-Ti diffraction patterns according to ICDD.

angle position may be understood from residual stresses within the film, but will not be evaluated here explicitly, because of the small precision in position measurement and the variation of diffraction vector orientation in the grazing incidence geometry. The metallic matrix phase was not detected, most probably because of its low concentration and its amorphous structure.

It can be seen from the figure that Bragg reflections caused from the TiO_2-layer exhibited a large broadening. In order to derive the grain size from this effect, peak profiles were fitted by pseudo Voigt model functions and the profile parameters like peak centroid $2\theta_0$, full width at half maximum (FWHM) 2ω and integral intensity I were determined. Grain sizes were evaluated by simply applying Scherrer's equation, $\langle L_V \rangle = 0.94\ \lambda / 2\omega \cos\theta_0$ [20], from which a volume-averaged column height $\langle L_V \rangle$ is obtained, which is a rough measure for the average grain size. Contributions of microstrain to the peak broadening were neglected, because the combined determination of grain size and microstrains requires a set of free standing, non-overlapping peaks to be evaluated, for instance, in terms of the Williamson–Hall scheme [21]. Since microstrains are mainly caused by dislocations, this approximation may be justified in the case of grains that are too small for dislocation to occur. It should be remembered that dislocation-induced strain fields usually extend over tens of nanometers [1], and that the dislocation core generally measures approximately 1 nm. The determination of $\langle L_V \rangle$ values for the diffractogram given in Fig. 5 were then found to lie between 2.4 and 7.8 nm. It is well known that the size averaging according to Scherrer's equation yields rather large values when compared with the median or mean value of diameters of grain populations [22]. The median of the diameter distribution function will accordingly be smaller than the values given above. It, therefore, appears appropriate to consider $\langle L_V \rangle$ values as upper limits for the grain size and it may safely concluded that the size of rutile grains in TiO_2-based coatings is less than 10 nm. This might also be taken as justification for neglecting the effect of dislocation-induced microstrain on peak broadening.

5. Discussion

In a recent work, Bendavid et al. have demonstrated the preparation of titanium dioxide films in the rutile modification by filtered arc deposition for which microhardness values up to 18 GPa could be obtained [23]. Such high hardness values could also be demonstrated by Bally et al. [24] and Lapostolle et al. [25] for TiO_2. We note, that these results for TiO_2 films clearly surmounted the bulk hardness of rutile, which is given as 1100 HV in the literature [1], but still differ from the 24 GPa obtained for the GFS-prepared films in this work. Bally et al. and Lapostolle et al. even succeeded in the preparation of hard TiO_x coatings in the 20–23 GPa range by reactive magnetron sputtering, but these films were suboxidic and deviated strongly from the ideal TiO_2 stoichiometry. Bally et al. reported that substoichiometric films were golden-metallic to dark blue and intransparent for optical wavelength. In a temper experiment with an as-deposited TiO_{1+x} film, the O content was varied to arrive at almost stoichiometric TiO_2, which was accompanied by a hardness drop from 23 to 21 GPa [24].

Regarding a possible explanation for the high hardness obtained we consider two different line of arguments by which the phenomenon may be understood. Firstly, the nanogranular morphology of the coatings may impede the occurrence and the motion of dislocation within the coatings [26]. The high hardness of the layers could then be understood in terms of a reduced dislocation mobility leaving any plastic deformability only to the comparatively more elaborate grain boundary displacement. It should be considered in this context, however, that the familiar Hall–Petch rule has to be modified when grain sizes in the nanometer range are considered [27]. The advantageous mechanical properties would accordingly be caused by the ability of the GFS technique to produce nanogranular particles. Secondly, the exceptional hardness of TiO_2-derived coatings prepared by GFS may be understood from the ion bombardment during growth. Ion currents at the substrate holder were specified during the deposition process by the bias generator that was run in the constant voltage mode. According to this measurement the ion current density amounted to 4–6 mA/cm^2 during the deposition of the oxide layer. These current densities indicate a strong ion bombardment when compared to other deposition experiments as performed by magnetron sputtering, for instance. It has to be remembered, however, that this large ion flux to the substrate is associated with ions of much lower energy when compared with other sputtering processes. This is due to the high pressure and the small average free paths of atoms and ions in the plasma of the gas-flow sputtering process, leading to a fast thermalisation of atoms and ions [28]. The ion bombardment would then be associated with a large number of ions, but of low energy. We conclude that both possible explanations of the high hardness—the nanometer-size hypothesis and the ion bombardment hypotheses—rely on the special conditions the growing film encounters during the GFS process.

It is of interest to compare the results of this work for TiO_2 with those obtained for other hard oxide coatings. High hardness values of up to 24 GPa have, for instance, been achieved in the case of Al_2O_3 prepared by pulsed magnetron sputtering [3] or pulsed d.c. PACVD processes [4]. But to arrive at hardness values of approximately 20–24 GPa the heating of the substrate to temperatures in excess of 600 °C and even more have

to be applied. The effect is understood from the several phases existing in the Al–O material system, from which only the high-temperature α-Al_2O_3 phase is suited for hard coatings, while the hardness associated with the amorphous and the γ-phase only amounts to values of 10 GPa or less than 20 GPa, respectively. For many mechanical working parts the thermal load associated with such high temperatures is undesired and hard TiO_2 coatings prepared at less than 200 °C would offer a useful technical alternative. Other applications for the titanium dioxide films presented here will be derived from their useful optical and electrically isolating properties. Most importantly, in contrast to the classical hard coatings from the nitride material system like TiN, AlN, etc., a hard TiO_2 coating is transparent for visible light. It, therefore, offers one of the very few technical solutions for a transparent coating for protection against scratching and abrasing loads, which is of technical importance for a large variety of applications.

6. Conclusion

In conclusion, it has been shown that nanocomposite coatings based on TiO_2 and Al_2O_3 as ceramic phase in combination with either Cu or W as metal matrix phase can be prepared by the GFS technique. The gas flow sputtering technique was demonstrated by capture experiments in combination with TEM of being capable to produce nanometer-sized particles by nucleation and growth of sputtered atoms during the transport from the target to the substrate. Prepared films were highly compact and contained few in- and ex-situ infiltrated contaminants. X-Ray diffraction revealed the titanium dioxide to exist mainly in the rutile phase with grain diameters of less than 10 nm. TiO_2-derived films turned out to be superior when compared to Al_2O_3-based ones and exhibited a high mechanical hardness up to 24.1 GPa and small wear coefficients under unlubricated sliding of 0.35×10^{-6} mm^3/Nm. These advantageous properties were achieved without intentionally heating the substrate under a low thermal budget regime.

Acknowledgments

This work was supported by the Bundesministerium für Bildung und Forschung (#03N3086B), Robert Bosch GmbH and Volkswagen A.G. We gratefully acknowledge the close cooperation with our industrial partners. We also thank Dr H. Bremers, T.U. Braunschweig, for help in XRD work, Dr U. Gernert, TU Berlin, for SEM micrograph, Dr S. Maas, M.A.S. Freiburg, for taking the TEM pictures, C. Steinberg for EPMA and P. Willich for SIMS investigation.

References

[1] M. Ohring, The Materials Science of Thin Films, Academic Press, San Diego, 1992, p. 12, Chapter 12 and Table 1.
[2] R.F. Bunshah, Handbook of Hard Coatings, William Andrew Publishing, Norwich, 2001.
[3] O. Zywitzki, G. Hoetzsch, Surf. Coat. Technol. 94–95 (1997) 303.
[4] C. Täschner, B. Ljungberg, V. Alfredsson, I. Endler, A. Leonhardt, Surf. Coat. Technol. 108–109 (1998) 257.
[5] A. Rosidian, Y. Liu, R.O. Claus, Adv. Mater. 10 (1998) 1087.
[6] J. Karch, R. Birringer, H. Gleiter, Nature 330 (1987) 586.
[7] T. Jung, A. Westphal, Surf. Coat. Technol. 59 (1993) 171.
[8] T. Jung, T. Kälber, V. von der Heide, Surf. Coat. Technol. 86-87 (1996) 218.
[9] K. Ishii, T. Ohba, T. Hara, Mater. Sci. Eng. A217-218 (1996) 232.
[10] M. Höfer, A. Jung, T. Jung, H.-U. Kricheldorf, F. Schmidt, 43rd Annual Technical Conference of the Society of Vacuum Coaters, Society of Vacuum Coaters, Denver, 2000.
[11] K. Ishii, J. Vac. Sci. Technol. A7 (1989) 256.
[12] T. Kälber, Hohlkathoden–Gasflußsputtern zur Verschleißschutzbeschichtung von Kunststoffen, Doctoral Thesis, TU Braunschweig, 1998.
[13] D.L. Peng, T.J. Konno, K. Wakoh, T. Hihara, K. Sumiyama, Appl. Phys. Lett. 78 (2001) 1535.
[14] W.C. Hinds, Aerosol Technology, Wiley, New York, 1999.
[15] Universalhärteprüfung-Teil 1: Prüfverfahren, Deutsches Institut für Normung, Berlin, 1997.
[16] H.-H. Behnke, Härt. Techn. Mitt. 48 (1993) 3.
[17] S. Veprek, Thin Solid Films 317 (1998) 449.
[18] J. Musil, J. Vlcek, Surf. Coat. Technol. 142-144 (2001) 557.
[19] M. Woydt, Tribol. Lett. 8 (2000) 117.
[20] B.E. Warren, X-Ray Diffraction, Addison-Wesley, Reading, 1969.
[21] J.I. Langford, D. Louer, E.J. Sonneveld, J.W. Visser, Powder Diffr. 1 (1986) 211.
[22] C.E. Krill, R. Birringer, Philos. Mag. A 77 (1998) 621.
[23] A. Bendavid, P.J. Martin, H. Takikawa, Thin Solid Films 360 (2000) 241.
[24] A.R. Bally, P. Hones, R. Sanjinés, P.E. Schmid, F. Lévy, Surf. Coat. Technol. 108-109 (1998) 166.
[25] F. Lapostolle, A. Billard, J. von Stebut, Surf. Coat. Technol. 135 (2000) 1.
[26] R. Hauert, J. Patscheider, Adv. Eng. Mater. 2 (2000) 247.
[27] D.A. Konstantinidis, E.C. Aifantis, Nanostruct. Mater. 10 (1999) 1111.
[28] K. Ishii, H. Hamakake, 43rd Annual Technical Conference of the Society of Vacuum Coaters, Society of Vacuum Coaters, Denver, 2000.